Conformational Changes in the Selectivity Filter of the Open-State KcsA Channel: An Energy Minimization Study

Gennady V. Miloshevsky and Peter C. Jordan
Department of Chemistry, Brandeis University, Waltham, Massachusetts

ABSTRACT Potassium channels switch between closed and open conformations and selectively conduct K^+ ions. There are at least two gates. The TM2 bundle at the intracellular site is the primary gate of KcsA, and rearrangements at the selectivity filter (SF) act as the second gate. The SF blocks ion flow via an inactivation process similar to C-type inactivation of voltage-gated K^+ channels. We recently generated the open-state conformation of the KcsA channel. We found no major, possibly inactivating, structural changes in the SF associated with this massive inner-pore rearrangement, which suggests that the gates might act independently. Here we energy-minimize the open state of wild-type and mutant KcsA, validating in silico structures of energy-minimized SFs by comparison with crystallographic structures, and use these data to gain insight into how mutation, ion depletion, and K^+ to Na^+ substitution influence SF conformation. Both E71 or D80 protonations/mutations and the presence/absence of protein-buried water molecule(s) modify the H-bonding network stabilizing the P-loops, spawning numerous SF conformations. We find that the inactivated state corresponds to conformations with a partially unoccupied or an entirely empty SF. These structures, involving modifications in all four P-loops, are stabilized by H-bonds between amide H and carbonyl O atoms from adjacent P-loops, which block ion passage. The inner portions of the P-loops are more rigid than the outer parts. Changes are localized to the outer binding sites, with innermost site S4 persisting in the inactivated state. Strong binding by Na^+ locally contracts the SF around Na^+, releasing ligands that do not participate in Na^+ coordination, and occluding the permeation pathway. K^+ selectivity primarily appears to arise from the inability of the SF to completely dehydrate Na^+ ions due to basic structural differences between liquid water and the "quasi-liquid" SF matrix.

INTRODUCTION

The *Streptomyces lividans* KcsA channel (1) selectively conducts K^+ across cell membranes, alternating between closed and open conformations in response to changes in cytosolic pH. Its pore, passing K^+ at near diffusion-limited rates, is ~170 times more permeable to K^+ than Na^+ (2). The narrow pore's extracellular part, lined with four arrays of carbonyl groups, is responsible for K^+ selectivity, and an intracellular conformational change of the four inner TM2 helices is involved in gating (1). KcsA channel gating reflects its ability to switch, in a stimulus-controlled way, between protein conformers that are permeable (open) or sterically constricted (closed) to passage of K^+. Despite numerous biophysical studies, the molecular details of ion selectivity and gating are incompletely understood (3). A major problem is that KcsA's SF also plays an important structural and dynamical role in gating (4–9). The open state in KcsA is not governed only by the intracellular gate (6)—the SF can block ion flow via an inactivation process (5). It has been found that inactivation of the KcsA channel (5) is similar in its kinetic behavior to C-type inactivation of voltage-gated K^+ channels (5,10,11). Thus, the intracellular gate can be structurally open while the channel remains functionally inactivated due to constriction of the SF (6). However, direct evidence linking intracellular gate opening to conformational changes in the SF remains elusive (7). The problem is to distinguish between direct effects due to residue mutations and indirect effects arising from allosteric changes (e.g., a change in the shape and activity of the protein) in other parts of KcsA (12).

The x-ray structure of KcsA shows the basic architecture of potassium channels (1,13). It is formed by four identical subunits with fourfold symmetry about a central pore containing an extracellular SF, a water-filled mid-membrane cavity and an intracellular constriction where the TM2 helices cross and form a tight helical bundle (1). In the open-state conformation of MthK (14), a distantly related potassium channel from *Methanobacterium thermoautotrophicum*, the TM2 helices are bent near a conserved glycine and splayed open, suggesting that a substantial outward hinge-bending movement is the main conformational change during gating. This large structural change is mainly confined to the intracellular half of the channel, leaving the extracellular half basically unaltered. A site-directed mass tagging technique (15) demonstrated that KcsA is a dynamically modular protein; the extracellular half remains rigid during gating, while the intracellular half undergoes a significant conformational change. These results show that the rigid scaffold surrounding the SF is maintained during gating and that the impact of the gating transition on filter structure is minimal. Normal mode analysis of KcsA's intrinsic structural flexibility (16) revealed that each TM2 helix pivots on the intrasubunit hinge, located about ⅓ of the helix's length from the extracellular side, and that the TM2 helical bundle rotates concertedly around the channel axis at the intracellular side. This intrasubunit hinge clearly distinguishes two dynamically separate domains: the

Submitted May 6, 2008, and accepted for publication June 25, 2008.

Address reprint requests to Peter C. Jordan. E-mail: jordan@brandeis.edu.

Editor: Richard W. Aldrich.

0006-3495/08/10/3239/13 $2.00

doi: 10.1529/biophysj.108.136556

more rigid SF including the P-helix, and the more mobile peripheral TM1 and TM2 helices. Thus, filter domain rigidity, which is essential for selectivity, is maintained during large-scale movement of the inner TM2 helical bundle around the channel axis. We recently modeled the acidified cytoplasm by protonating the TM2 C termini and then generated the open-state conformation of KcsA in silico using the Monte Carlo normal mode following (MC-NMF) method (17). When viewed from the cytoplasm, the gating transition in KcsA involves clockwise rotation and unwinding of the TM2 bundle, lateral movement of the TM2 helices away from the channel axis, and transformation of the narrow hydrophobic vestibule into a very wide domain, fully integrated with the intracellular solution. Recent experiments (18) in which a gold nanocrystal was attached to the cytoplasmic KcsA domain unambiguously showed that upon cytoplasmic acidification, the channel opens and the transmembrane helices rotate clockwise (viewed from the cytoplasmic side; see Fig. 7 of Shimizu et al. (18). Rotational motions around the channel's longitudinal axis predominated and far exceeded the radial expansion of the inner helices. At pH 4.0 rotational motion was identified as originating from the TM domain (18), where the pH sensor is presumably located, confirming our prediction of how charged residues near the C termini of TM2 affect KcsA gating (17). We found that in the open state of KcsA (17), only the narrow 12-Å long SF constitutes the pore. The central cavity and inner pore characteristic of the closed state disappeared and were rearranged into a wide cytoplasmic vestibule. The SF P-loops were essentially unaffected during the gating process (Supplementary Material, Movie S1 and Data S2). Both experiment and theory suggest that the SF and the intracellular helix bundle might act independently. The TM2 helical bundle is the primary gate of KcsA, while structural rearrangements at the SF act as the second gate, obstructing ion flow even with an open bundle crossing (6,7).

In our MC-NMF simulations generating the splayed-open-inner pore (17), the SF underwent no crucial structural change that could account for inactivation. We can thus hypothesize that inactivation reflects local conformational changes in the SF associated, e.g., with modifying the H-bonding network behind the P-loops or potassium occupancy of the SF. Consequently, our goal is to computationally predict mutant protein structures and local structural changes due to substitutions, insertions, or deletions of residues, waters, and ions in the SF of open-state KcsA. Put somewhat differently, one can use theory to take structural snapshots in a way mimicking that done crystallographically, thereby predicting (resolving) mutant protein structures. One approach to this goal is via molecular dynamics (MD) simulation (19). However, MD trajectories trace highly complex molecular motions, exhibiting substantial ''simulational noise.'' The protein's flexibility and the generally large atomic fluctuations make it very difficult to extract the microscopic origin of physical phenomena, such as ion selectivity, from all-atom MD. Trajectories do not yield well-tuned, clearly identifiable structures, but describe a fluctuating protein undergoing small-scale conformational transitions. Thermal fluctuations cause the simulated protein to deviate from the crystal structure, complicating comparison with experiment. Thus, it can be very difficult to interpret motions and snapshots taken at arbitrary times along an MD trajectory. Therefore, MD does not really suit our purposes. Instead, we propose to address the structural problem via energy minimization (20). Why should this work? Mutations in the SF domain leave the inner pore unaffected, and adjustments in the protein's native-fold are generally small and deviate only slightly from the crystallographic structure. A case in point is an E71A-Fab mutant that was captured in two conformations (6). One was quite similar to WT KcsA, whereas the other clearly differed, exhibiting local changes in three regions of the outer pore: the P-loops, the pore mouth D80, and W67 along the pore helix. However, even here there were no resolvable cytoplasmic changes, again suggesting that outer pore behavior is effectively decoupled from the inner pore region (7). In modification of the outer pore conformation, the remainder of the protein undergoes no major repacking. Consequently, an energy-minimized mutant's final conformation is also a snapshot of a low-temperature configuration, similar in every way to one determined crystallographically. Thus, mutant structural refinement is performed relative to low-temperature data with local adjustments at mutation sites. Energy minimization fine-tunes (refines) the location, the optimal geometry, and the energy of the mutant protein's preferred conformation, data that we can immediately use to compare with and interpret experimental results.

Here, we apply energy minimization to study SF conformations. Our arguments are based on a basic hypothesis: structural change in the SF is essentially uncoupled from that occurring in the cytoplasmic half of the channel assembly. We can thus use closed-state SF data to check the reliability of open-state SF conformations established in silico. The aim is to 1), validate energy-minimized open-state KcsA variants by comparison with available crystallographic data; and 2), gain insight into how the SF structure responds to protonation, ion depletion, and K^+ to Na^+ substitution.

MATERIALS AND METHODS

We base our energy minimizations on an all-atom model of the open-state KcsA channel (17) embedded in an explicit lipid bilayer and solvated by water molecules. This open-state KcsA structure, generated by our MC-NMF simulations (17), corresponds to a high-energy state. A side view of the central simulation cell showing the open-state structure of KcsA, potassium ions, dipalmitoyl phosphatidylcholine (DPPC) lipids, and water molecules is shown in Fig. 1 (see online version for color Figs. 1–5). Periodic boundary conditions were applied in all directions. The purpose of the large solvent box was twofold: first, to stabilize polar and charged residues on the surface of the KcsA protein; second, to account for the effect of surroundings on conformations of the SF. The central cavity is now an integral part of the cytoplasm, forming an intracellular vestibule. About ~400 water molecules are located in this region, which still binds a cation at the former cavity site, near the

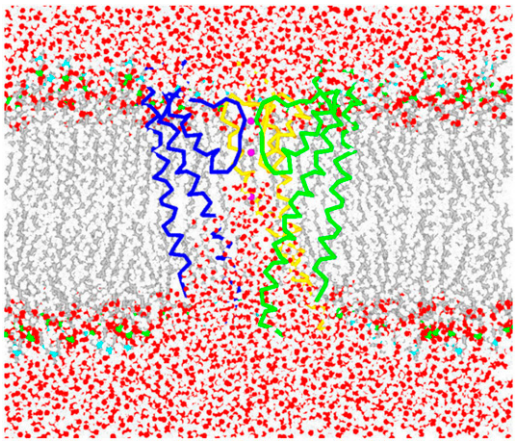

FIGURE 1 Side view of the central simulation cell showing open-state KcsA, 3 K^+ ions, 123 DPPC lipids, and ~7000 waters (~400 in the intracellular vestibule). Three KcsA subunits are shown in backbone representation in green, blue, and yellow colors. Lipid head groups are shown in native colors. For clarity, fronting lipids and one KcsA subunit are not displayed. K^+ ions are depicted as pink spheres. Figs. 1–4 and 6 were generated using our MCICP code (21). (See online version for color Figs. 1–5.)

cytoplasmic exit of the SF. In what follows we refer to this open-state locus as a vestibule site.

The molecular system was described with the all-hydrogen CHARMM22 topology and parameter set (22). The Coulomb energy was calculated by a parallelized fast multipole method (23). The salt (Na^+-Cl^- electrolyte) was not included because the fast multipole method, properly accounting for long-range electrostatic effects, does not require artificial neutralization of the central simulation cell. Chloride ions are excluded from both the outer mouth (due to four negatively charged D80 and outward pointing carbonyl dipoles of the P-loops) and the vestibular binding site (due to the P-helix dipoles) (24). Minimizations were performed using the steepest descent method (20) and a new conjugate gradient method with guaranteed descent (25). The molecular system is unconstrained and all degrees of freedom (bond lengths, bond angles, torsion, and improper torsion angles) in KcsA, lipids, and waters vary freely. We mutate the SF and then minimize the assembled system using the steepest descent method with a random step length (20) to remove bad contacts and relax the molecular system; this takes ~500–1000 steps. We perform a number of minimization runs on the same initially assembled molecular system using this ''arbitrary step'' minimization approach (20). Each minimization run effectively generates different final configuration due to a random step length used in the steepest descent method. This allows us to identify how the system changes from one minimum energy structure to another, how the relative positions of the atoms vary, and what structural changes occur. Because the focus of this study is only the conformational states of the SF P-loops and H-bonding network, this approach can produce similar or different SF configurations separated by energy barriers. Finally, the various molecular systems (different starting points) generated by applying the steepest descent method (20) were well tuned using the conjugate gradient method with guaranteed descent (25).

RESULTS

Previous work showed that if the E71-D80 proton bridge in the SF is maintained, the P-loops remain structurally intact during channel opening (17). Since the P-loops are not perturbed in transition to the open state, the closed-state crystal structure (13) (pdb code 1K4C) of the SF can be used as a reference state for assessing structural changes in response to mutation, K^+ depletion, or Na^+ substitution in the SF of open-state KcsA. We now describe various KcsA modifications and, by comparing their SF domains with appropriate crystallographic data, demonstrate the physical relevance of the minimized structures.

Confirming the high [K^+] conformer open-state SF structure of KcsA, based on 1K4C

Our open-state KcsA (17) was generated for an SF occupancy scenario corresponding to the high [K^+] conformation, 1K4C (13). Fig. 2 directly contrasts crystal closed-state (13) and minimized open-state (17) SF structures, with (Fig. 2 *a*) and without (Fig. 2 *b*) a water molecule behind the P-loop. In each case we protonate the E71 side chains (E71p) consistent with considerable evidence: this residue's immediate environment is nonpolar; when protonated in silico, KcsA simulations

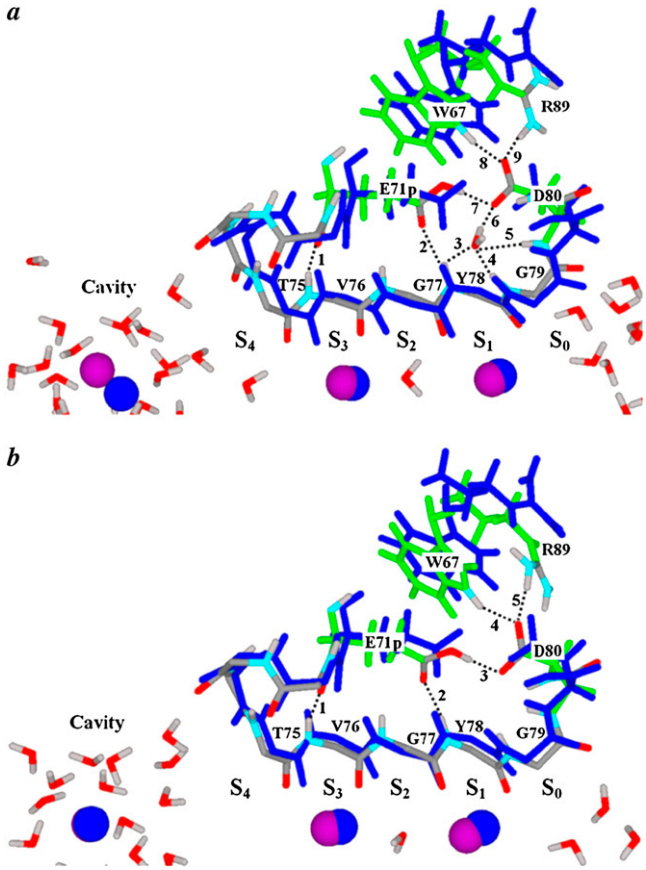

FIGURE 2 Conformations of the SF of closed- (high-[K^+] structure, 1K4C in blue) and open-state (energy-minimized KcsA, native colors) structures for protonated E71 and deprotonated D80, (*a*) with and (*b*) without a water molecule behind the P-loop. The three K^+ ions in the pore at their crystal locations are illustrated in blue. SF residues of only one subunit are displayed. Filter residues are labeled near their carbonyl ends. Backbone atoms are only shown for residues 72–79. Side chains of E71, D80, R89, and W67 (energy-minimized KcsA) are shown in green, with atoms participating in H-bonding shown in native colors.

reproduce crystal data; when they are not, there is a significant D80-E71 repulsion and the SF distorts severely (26,27). SF P-loops are stabilized by H-bonds between amide hydrogens (Hs) of V76 and Y78 and carbonyl and carboxylate oxygens (Os) of E71 (Fig. 2, *dashed lines 1* and *2*). Amide Hs of neither G77 nor G79 are bonded in Fig. 2 *b*, but the amide H of G79 is structurally constrained by H-bonding to water in Fig. 2 *a*. An H-bond forms between the protonated carboxylate O of E71 (Fig. 2 *a*, *dashed line 7* and Fig. 2 *b*, *dashed line 3*) and one of the carboxylate Os of D80. The other D80 carboxylate O forms H-bonds with the aryl HE1 of W67 and Hs of R89. The R89s are from adjacent subunits; their side chains rearrange and H-bond with D80. Table 1 quantitatively characterizes these interactions. All but two of the 11 putative H-bonds are short, with their X-H-Y triads nearly collinear, indicating a robust, highly-organized network. Relative to the SF of 1K4C, the root mean-square deviation (rmsd) for backbone Cα values of the P-loops is $<$0.5 Å. The conformation of an energy-minimized SF with the salt bridge formed from D80p/E71 (protonating D80 and ionizing E71; not shown) very closely resembled both crystal and E71p/D80 structures. A number of minimizations starting from different initial conditions led to the same final SF conformation.

Conversely, when both E71 and D80 are charged, there is significant SF rearrangement due to mutual repulsion. Differences in the H-bonding network involving E71, D80, and R89 are shown in Fig. 3, *a–d*. The D80 side chain moves toward the periplasm and is stabilized by H-bonding to the neighboring subunit's R89 and/or aryl HE1 of W67 (Fig. 3, *a–d*). In one case (Fig. 3 *d*) the R89 side chain directly mediates interaction between E71 and D80. The E71 side chain is stabilized by H-bonds with amide Hs of the P-loop, the aryl HE1 of W67, and a water molecule. With a water molecule behind the P-loops (Fig. 3, *a* and *b*), the P-loop conformation mimics that of the crystal structure. Without this water molecule (Fig. 3, *c* and *d*), the binding site S1 reconfigures:

TABLE 1 Structural parameters of the H-bonding network behind the SF P-loops for the energy-minimized open-state high [K^+] structure of KcsA (Fig. 2 *a* and *b*)

H-bond lengths, Å		H-bond angles, degree	
(HN)T75-(O)T72	2.2	(O)T72-(HN)T75-(N)T75	145
(HN)V76-(O)E71p	1.8	(O)E71p-(HN)V76-(N)V76	162
(HN)G79-(OH2)H_2O*	1.8	(OH2)H_2O-(HN)G79-(N)G79*	163
(HN)D80-(OH2)H_2O*	2.7	(OH2)H_2O-(HN)D80-(N)D80*	121
(HN)Y78-(OE1)E71p	2.0	(OE1)E71p-(HN)Y78-(N)Y78	161
(HN)G77-(OE1)E71p	2.5	(OE1)E71p-(HN)G77-(N)G77	126
(H2)H_2O-(OD1)D80*	1.7	(OH2)H_2O-(H2) H_2O -(OD1)D80*	172
(HN)L81-(OD1)D80	2.1	(OD1)D80-(HN)L81-(N)L81	147
(HE2)E71p-(OD1)D80	1.7	(OE2)E71p-(HE2)E71p-(OD1)D80	166
(HE1)W67-(OD2)D80	1.8	(OD2)D80-(HE1)W67-(NE1)W67	159
(HH21)R89-(OD2)D80	1.7	(OD2)D80-(HH21)R89-(NH2)R89	175

Bonds and angles are grouped according to HB acceptor type. CHARMM conventions are used.

*H-bonds involving the structural water in Fig. 2 *a*.

the Y78-G79 peptide plane bends away from the channel axis due to interaction with E71, thus opening S1 to the periplasm with the S1 K^+ solvated by at least two waters. Due to the increased negative charge (an additional $-4e$) in the SF, the vestibular K^+ moves ~2.2–3.9 Å nearer the SF. Slightly different H-bonding patterns, other than those shown in Fig. 3, *a–d*, were observed in minimizations with different initial conditions.

Confirming the low [K^+] conformer open-state SF structure of KcsA, based on 1K4D

We now modify SF occupancy of open-state KcsA with E71p (17) to mimic that observed in the low-[K^+] structure, 1K4D (13), where the P-loop is highly distorted as compared to the high [K^+] structure. Guided by 1K4D, in our new starting structure site S2 is vacant, site S3 is occupied by a water molecule, K^+ occupies both sites S1 and S4, and Na^+ is in the vestibule (Fig. 4 *a*). Further mimicking the crystal, two water molecules are placed behind the P-loop (13). After minimizing this modified open-state KcsA, the conformation of the SF closely resembles that of 1K4D. R89 moves toward D80, forming a salt bridge. One carboxylate O of D80 forms H-bonds with the aryl HE1 of W67 and Hs of R89 (*dashed lines 9* and *10*). The carbonyl O of E71p remains H-bonded with the V76 amide H. The two water molecules behind the P-loop form an H-bonded network with amide Hs of G79 and Y78 and carboxyl Os of E71 and D80. The corresponding H-bonding parameters are reported in Table 2 and again suggest the presence of a robust, highly organized H-bond network. The SF conformations illustrated in Fig. 4 *a* and Fig. 2 *a* differ notably. In Fig. 2 *a*, one carboxylate O of E71 is H-bonded to the amide H of Y78. However, Fig. 4 *a* indicates that structural coupling of carboxylate Os of E71 and D80 with amide Hs of the SF P-loop is indirect, occurring only in response to mediation by the water molecules. In comparison to the high [K^+] conformation, this region of the SF is congested (Fig. 4 *a*).

Confirming the SF structure of E71A KcsA, based on 1ZWI

Cordero-Morales et al. (6) reported two crystal structures of Fab stabilized KcsA with its E71 mutated to alanine (E71A). The P-loop of one of them, the so-called nonflipped structure, pdb code 1ZWI, is shown in Fig. 4 *b*. An energy-minimized E71A-KcsA structure is superposed. In 1ZW1, ion occupancy of S1-S3 and of S2-S4 was approximately equally likely (6). Fig. 4 *b* illustrates the structural consequences of minimization if both sites S1 and S3 are occupied by K^+ and water molecules occupy sites S2 and S4; SF structure was little altered for minimization runs with the ions at S2 and S4 and the waters at S1 and S3 (data not shown). A water molecule is located behind the P-loop. The R89 side chain moves toward D80, forming a salt bridge. The conformation

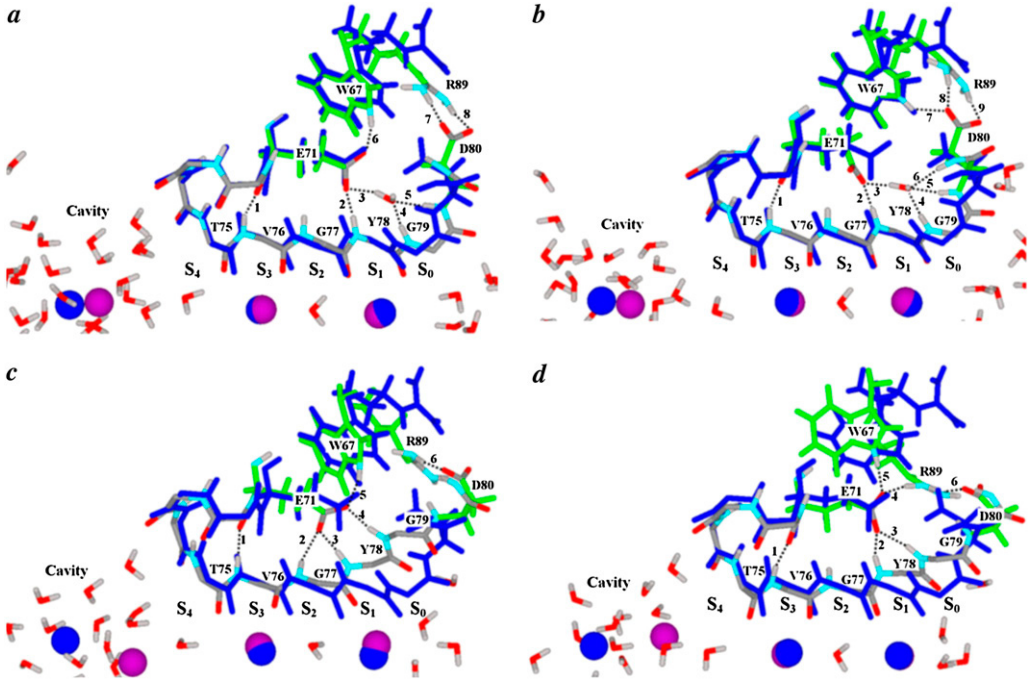

FIGURE 3 Conformations of the SF of closed- (high-[K^+] structure, 1K4C in blue) and open-state (energy-minimized KcsA, native colors) structures for both E71 and D80 ionized, (*a* and *b*) with and (*c* and *d*) without a water molecule behind the P-loop, respectively. The location of K^+ ions and filter waters, the residue labeling, and the color scheme are as in Fig. 2.

of D80 resembles that of the E71p structure (Fig. 2, *a* and *b*) and differs from those with both E71 and D80 charged (Fig. 3 *a–d*). The central part of the P-loop behind the SF is not H-bond stabilized: the amide H of G77 is unbound and the amide H of Y78 binds weakly to the water O (*dashed line 2*, H-bond length 2.5 Å, Table 3). The water O stabilizes the amide H of G79 (*dashed line 3*). A water molecule stabilizes one carboxylate O of D80 (*dashed line 4*); the other carboxylate O forms H-bonds with the aryl HE1 of W67 and H atoms of R89 (*dashed lines 5* and *6*). The H-bonding parameters reported in Table 3 again indicate a well-articulated H-bond network. For this nonflipped structure, minimization runs starting from different initial conditions led to the same final conformation of the SF P-loops.

TABLE 2 Structural parameters of the H-bonding network behind the SF P-loops for the energy-minimized open-state low [K^+] structure of KcsA (Fig. 4 *a*)

H-bond lengths, Å		H-bond angles, degree	
(HN)T75-(O)T72	2.7	(O)T72-(HN)T75-(N)T75	127
(HN)V76-(O)E71p	2.4	(O)E71p-(HN)V76-(N)V76	152
(HN)Y78-(OH2)H_2O	2.1	(OH2) H_2O -(HN)Y78-(N)Y78	134
(HN)G79-(OH2)H_2O	2.1	(OH2)H_2O-(HN)G79-(N)G79	170
(H2)H_2O-(OH2)H_2O	1.8	(OH2) H_2O-(H2)H_2O-(OH2)H_2O	160
(HN)D80-(OH2)H_2O	2.4	(OH2)H_2O-(HN)D80-(N)D80	134
(H1)H_2O-(OE1)E71p	1.7	(OE1)E71p-(H1)H_2O-(OH2)H_2O	172
(H2)H_2O-(OD1)D80	1.7	(OD1)D80-(H2)H_2O-(OH2) H_2O	172
(HN)L81-(OD1)D80	1.8	(OD1)D80-(HN)L81-(N)L81	155
(HE2)E71p-(OD1)D80	1.7	(OD1)D80-(HE2)E71p-(OE2)E71p	173
(HE1)W67-(OD2)D80	1.9	(OD2)D80-(HE1)W67-(NE1)W67	157
(HH22)R89-(OD2)D80	1.9	(OD2)D80-(HH22)R89-(NH2)R89	144
(HH11)R89-(OD2)D80	1.8	(OD2)D80-(HH11)R89-(NH1)R89	151

Bonds and angles are grouped according to HB acceptor type. CHARMM conventions are used.

Conformations of an empty SF

Here we removed both ions and waters from the SF and minimized the new open-state of KcsA. SF flexibility, under these extreme conditions, is illustrated in Fig. 5. The channel remains intact, but peptide planes undergo strong concerted distortions and flipping. The distorted SF is effectively stabilized by an H-bond network between amide Hs and Os from adjacent P-loops. In Fig. 5 *a* (E71p protonation state), the structure of the SF is highly deformed from the extracellular vestibule to the V76 residues; it differs substantially from the highly organized cylindrical geometry of the 1K4C pore, where all carbonyl Os from the four P-loops point toward the filter axis (see Fig. S1 in Data S1). The Y78-G79 peptide planes, at the exterior entrance to the SF, are distorted by ~90°. The α-carbons of G77, in the center of the SF, twist inward, occluding the pore. Peptide-plane flip of ~90–180° is observed for G77-Y78 and V76-G77. The peptide planes of T75-V76 exhibit little distortion. Their carbonyl O atoms remain pointed toward the pore axis. The rmsd is 0.83 Å for α-carbons and 1.0 Å for the whole KcsA structure relative to the energy-minimized open-state high [K^+] structure of Fig. 2 *a*. In contrast, the SF of the E71A mutant (Fig. 5 *b*) is far

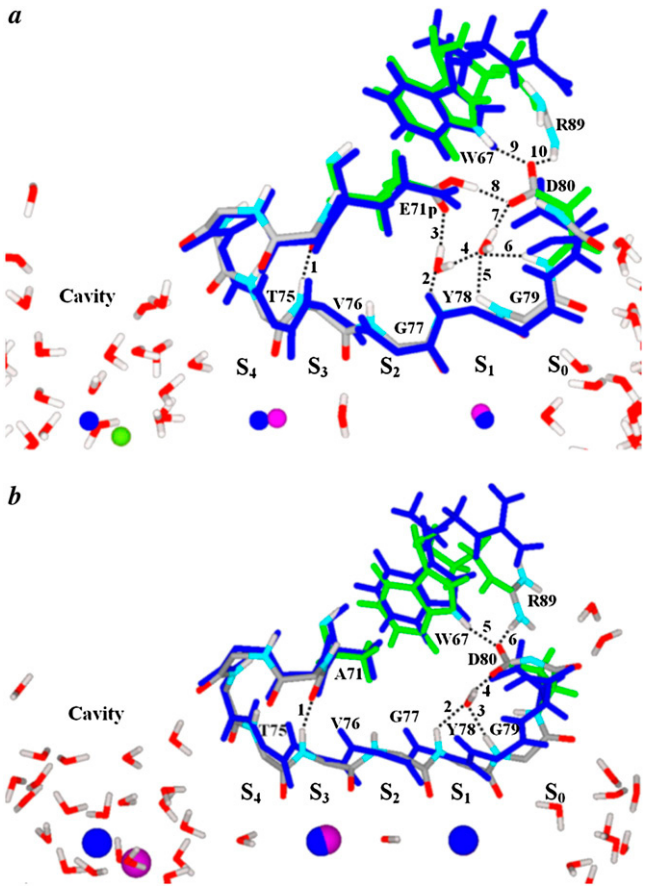

FIGURE 4 Conformations of the SF of (*a*) closed low [K^+] (1K4D, *blue*) and open-state energy-minimized E71p KcsA (*native colors*) and (*b*) closed nonflipped E71A KcsA (1ZWI, *blue*) and open-state energy-minimized E71A KcsA (*native colors*) structures. (*a*) Site S2 is vacant and two water molecules are located behind the P-loop; K^+ (*purple*) occupies sites S1 and S4, with Na^+ (*green*) in the cavity. (*b*) Blue spheres represent the cavity, and S1 and S3 binding sites of 1ZW1; in the minimized structure, K^+ (*purple*) occupies these sites.

less deformed than that of the E71p KcsA variant (Fig. 5 *a*). H-bonding with water molecules at the extracellular mouth stabilizes peptide planes of Y78-G79, which is not seen in Fig. 5 *a* (the E71p variant). The only highly distorted regions

TABLE 3 Structural parameters of the H-bonding network behind the SF P-loops for the energy-minimized open-state E71A structure of KcsA (Fig. 4 *b*)

H-bond lengths, Å		H-bond angles, degree	
(HN)T75-(O)T72	2.7	(O)T72-(HN)T75-(N)T75	116
(HN)V76-(O)A71	1.9	(O)A71-(HN)V76-(N)V76	153
(HN)Y78-(OH2)H_2O	2.5	(OH2) H_2O -(HN)Y78-(N)Y78	119
(HN)G79-(OH2)H_2O	1.9	(OH2)H_2O-(HN)G79-(N)G79	168
(H2)H_2O-(OD1)D80	1.6	(OD1)D80-(H2)H_2O-(OH2)H_2O	168
(HN)D80-(OD1)D80	2.2	(OD1)D80-(HN)D80-(N)D80	120
(HN)L81-(OD1)D80	1.8	(OD1)D80-(HN)L81-(N)L81	154
(HE1)W67-(OD2)D80	1.8	(OD2)D80-(HE1)W67-(NE1)W67	155
(HH21)R89-(OD2)D80	1.6	(OD2)D80-(HH21)R89-(NH2)R89	174

Bonds and angles are grouped according to HB acceptor type. CHARMM conventions are used.

are the G77-Y78 peptide planes (Fig. 5 *b* and Fig. S2 in Data S1). The peptide planes of V76-G77 and T75-V76 undergo little distortion; their carbonyl O atoms remain pointed toward the pore axis.

Conformations of an SF loaded with Na^+

Computed structures for an SF loaded with Na^+ are shown in Fig. 6, describing structural expectations for KcsA comparable to what would be found crystallographically. Three Na^+ replaced the K^+ originally located at the S1, S3, and vestibule sites; the system was then minimized. During minimization the protein and waters in the vicinity of the Na^+ reorganize and the ions move significantly. Atoms of the ions' first solvation shell are the most noticeably affected. The TM1, TM2, and pore helices exhibit little structural change due to replacement of K^+ by Na^+. Fig. 6 illustrates the conformation of the SF and the location of Na^+ for the E71p protonation variant (Fig. 6 *a*), and for the variant with both E71 and D80 ionized (Fig. 6 *b*). The rmsd is only 0.16 Å for α-carbons and 0.2 Å for the whole KcsA structure relative to the comparable energy-minimized structure occupied by K^+ (Fig. 2 *a*). The SF rearranges to bind the smaller Na^+. The ions either move from the center of S1 and S3 toward a ring of carbonyl Os, becoming solvated by four carbonyl Os and a water molecule (Fig. 6, *a* and *b*), or the original eight-carbonyl O cage deforms, with five Os collapsing around Na^+ (Fig. 6 *b*), in which case three carbonyl O atoms (*1*, *2*, and *3* in Fig. 6 *a*) do not directly coordinate Na^+. In the E71A mutant the SF conformation mimicked that of the E71p variant; both Na^+ ions are solvated by the ring of carbonyl Os and a water molecule (data not shown).

Strain energy for the molecular system with K^+ and Na^+ in the KcsA pore

Our reference is the energy-minimized structure of open-state E71p KcsA, embedded in the lipid-water environment, with three K^+ ions and water molecules in the pore. The strain energy is defined as the energy difference between conformations of equivalent molecular systems loaded with either K^+ or Na^+. The source of strain is quantified by examining the different components, Δ, as shown in Table 4. Δ_{tot} refers to energy differences for the entire system, and $\Delta_{ion} = \Delta_{tot}/3$ to per ion differences. Whereas the three binding sites differ, the Δ_{ion} values are still informative. From Table 4 we see that 1), the total energy of the molecular system loaded with Na^+ is substantially lower (~50 kcal/mol) than that with K^+, corresponding to a total energy difference per ion of approximately −16.5 kcal/mol; 2), the difference in the total nonbonded energy per ion, $\Delta_{ion} = -19.7$ kcal/mol, is comparable to the difference in hydration free energies between Na^+ and K^+ in bulk solution, approximately −18 kcal/mol (29–31). Thus, there is an unfavorable structural strain due to the total bond energy per ion (~3.2 kcal/mol), making the total energy difference per ion more positive (approximately

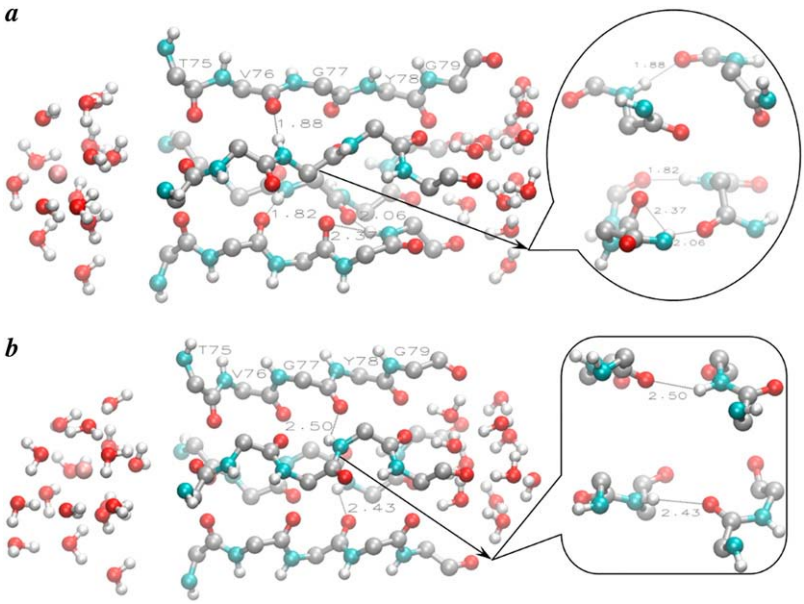

FIGURE 5 The energy-minimized structure of the four P-loops, void of K^+ and waters, in the SF of (*a*) E71p KcsA and (*b*) E71A KcsA. Only the backbone (CA, C, O, N, and HN) atoms of the P-loops are shown (*native colors*). To provide the impression of depth, a fog effect is employed, with above plane atoms brightest and lower ones faded to a background color. H-bonds stabilizing these conformations are shown as dashed lines and distances are labeled. K^+ occupies the cytoplasmic vestibule and waters are shown in the cytoplasmic vestibule and exterior mouth. The H-bonds between adjacent P-loops are shown in the enlarged insets with the view along the channel axis as seen (*a*) from the periplasm for E71p KcsA and (*b*) from the cytoplasm for E71A KcsA. The figure is drawn using VMD (28).

−16.5 kcal/mol). Energy minimization does not include entropy. However, entropic contributions to the free energy difference between K^+ and Na^+ nearly cancel at 300 K (30–35). Free energy contributions at 300K, due to entropy differences between ions in small aqueous clusters, were estimated as ~0.1 kcal/mol (32). Exhaustive analysis of experimental hydration energetics also indicates that entropic influences on the free energy difference are small (~0.25 kcal/mol) (34,35). MD simulations for a model of the pore's 8-coordinate carbonyl binding cavity also suggest that the entropy change per ion between states with K^+ and Na^+ is small, corresponding to 300 K free energy differences of less than ~1 kcal/mol (30,31). Thus, the total system energy is the major determinant for free energy differences between K^+ and Na^+ in KcsA binding sites.

DISCUSSION

Structural response of the KcsA SF to mutations

We found that SF P-loops are structurally unaffected by opening of the intracellular gate (17). Although the P-helices execute a small swinging motion associated with opening the TM2 bundle, this reflects a lever-like swinging of both TM2 and TM1 helices about pivot points near the C termini of the

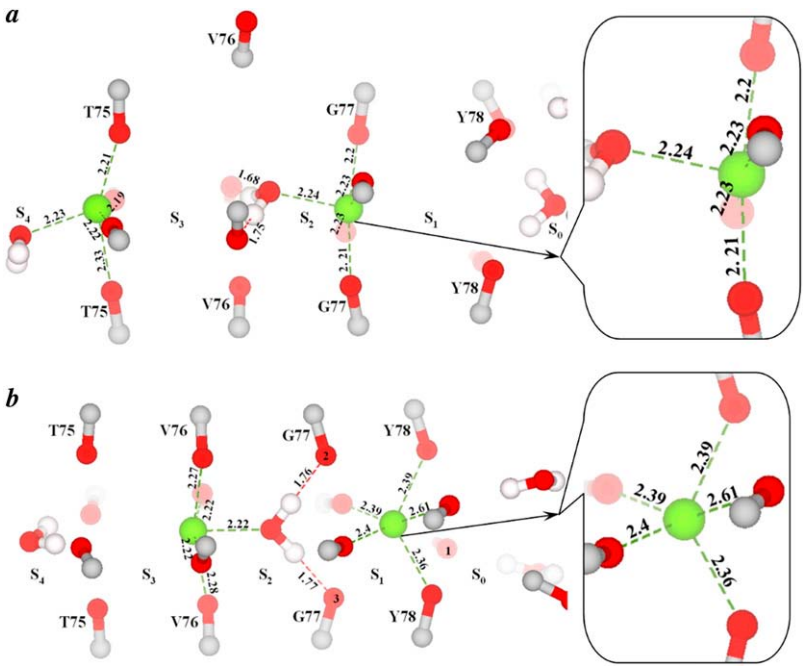

FIGURE 6 The energy-minimized SF loaded with Na^+ for two protonation variants: (*a*) E71p and (*b*) both E71 and D80 charged. Waters, Na^+, and carbonyl Os from the four P-loops are shown. To provide the impression of depth, the fog effect is employed, with above plane atoms brightest and lower ones faded to a background color. Sodium-oxygen bonds are shown as dashed lines and distances are labeled. One of the carbonyl Os of V76 in *a* has flipped. The distance between sodium and O atoms with labels 1, 2, and 3 in *b* is larger than 2.8 Å, and coordination is five-fold. The insets present enlarged pictures of fivefold coordination by (*a*) water O and a ring of four carbonyl Os and (*b*) five carbonyl Os.

TABLE 4 Strain energy difference for the E71p system with Na^+ and K^+ occupying the pore

Energy component	Δ_{tot}† kcal/mol	Δ_{ion}‡ kcal/mol
Electrostatic	−65.55	−21.85
van der Waals	6.41	2.14
Total nonbonded	*−59.1*	*−19.7*
Bond	1.19	0.397
Angle	4.89	1.63
Urey-Bradley angle	0.0945	0.0315
Dihedral	3.11	1.037
Improper	0.419	0.1397
Total bonded	*9.7*	*3.23*
Total	*−49.44*	*−16.48*

†Δ_{tot} is the strain energy difference for the entire system.
‡$\Delta_{ion} = \Delta_{tot}/3$ is per ion strain energy difference.

P-helices (16,17); all four SF P-loops remain intact, fluctuating slightly in space as a rigid unit (Movie S1 and Data S2). Therefore, closed-state x-ray structures of the SF can be utilized as templates for assessing structural responses. Energy minimization of open-state KcsA is used to identify protonation- or mutation-induced conformational changes in the SF relative to x-ray templates. We find that open-state structural changes due to protonation of E71 or D80, and replacement of side chains such as E71 by A71 can all be characterized as local SF-domain adjustments rather than perturbations requiring major repacking of KcsA.

The energy-minimized, open-state conformations of E71p variants correspond closely to the available crystal data. Differences in detail are inevitable, probably reflecting the approximate nature of biomolecular force fields. The SF of the energy-minimized E71p structure reorganizes and adjusts insignificantly when compared to the SF of the crystallographic structure (Fig. 2, *a* and *b*). The K^+ in the SF and the vestibule are only slightly displaced from their crystallographic positions. In the energy-minimized SF, both E71p and D80 side chains remain very close to their crystallographic locations, again strongly supporting the idea that they share a proton. A recent first-principles QM/MM MD study demonstrates proton exchange between these residues on a picosecond timescale, with a slight preference for E71 (36). In contrast, repulsive interaction between the E71 and D80 side chains in their default (ionized) protonation states leads to significant reorganization of the SF (Fig. 3, *a–d*). The E71 side chain bends, forming H-bonds between its carboxylate O atoms and amide Hs of G79, Y78 and/or G77 of the P-loop. Similar behavior was observed in MD simulations of KcsA with both E71 and D80 side chains fully ionized (26). The SF was significantly distorted and widened on the extracellular side (26) reminiscent of our observations (Fig. 3, *a–d*). A fully solvated Na^+, surrounded by six waters, was found at the widened site S1 (27).

Good agreement between the open-state E71p KcsA structure (17) and the crystallographic low-[K^+] structure, 1K4D (13) (Fig. 4 *a*), was found for only a few minimizations. In all runs, the P-loop conformation was distorted relative to 1K4C, but in many cases the peptide planes were tilted somewhat differently than in 1K4D. Quite possibly, the low-[K^+] crystal (1K4D) provides a snapshot of a particular distorted conformation of the SF.

Comparing our energy-minimized E71A with the nonflipped E71A KcsA (6) demonstrates good overall structural agreement for the P-loops and the A71, D80, and W67 side chains (Fig. 4 *b*). However, energy minimization led to no conformations similar to the flipped crystal structure of E71A KcsA, pdb code 2ATK (6). In this highly distorted flipped mutant, the side chain of D80 is oriented extracellularly, the side chain of W67 is found in two rotameric states, carbonyl Os of V76 and Y78 are directed away from the pore, and the position of the binding sites is displaced. This E71A structure has been postulated to be an intermediate conductive conformation (6). If so, it implies that the SF pore must be highly distorted by flipping carbonyl groups during the K^+-water translocation between binding sites.

Energy minimizing open-state KcsA under appropriate initial SF occupancies by K^+ and water leads to SF conformations in good agreement with available crystallographic structures and provides valuable insight into mutation-induced conformational changes in the SF. The starting conformation for the SF P-loops was the same as that in the crystal high-[K^+] KcsA structure, 1K4C (13), because we found no structural changes in the SF domain during the opening of the intracellular helical bundle (17). As seen in Figs. 3, *c* and *d* and 4 *a*, the introduction of protonations, mutations, or ion depletions in the SF domain, and the application of the ''arbitrary step'' and conjugate gradient minimization approaches (20,25), lead to final P-loop conformations that differ quite substantially both structurally and energetically from the initial cylindrical geometry of the 1K4C SF pore. This illustrates that energy barriers are crossed during minimization and that the final structures are trapped in states structurally and energetically different from their initial configurations. We find that the H-bonding network stabilizing amide Hs of the P-loops is sensitive to E71 mutations as well as to the presence of protein-buried water molecule(s). NMR spectroscopy provides direct confirmation, showing that the complex H-bond network between E71, D80, Y78, and G79 is a pH-sensitive trigger involved in SF gating (8). Buried water molecules are structural elements stabilizing the SF. Thus, many different SF conformations associated with different conformational states of the H-bonding network are possible.

Flexibility of the SF and inactivation

Occasional distortion of the SF, involving some carbonyl reorientation, has been seen in MD simulations (4,37–40). Under low [K^+] conditions, a distorted SF conformation with flipped peptide groups was reported in MD studies of Kir6.2 (37) and KirBac1.1 (38). To prevent such flipping, artificial harmonic constraints on SF carbonyl groups were used in

simulating K^+ conduction through Kv1.2 (39). Spontaneous flipping of a single V76-G77 peptide linkage, for a pore fully loaded with K^+, was observed in earlier MD studies of KcsA (40). The same MD simulational runs (4) based on the CHARMM force field, predicted that transition from the conducting state of the SF to the nonconducting state begins by an ~180° flip of the V76-G77 peptide linkage (40) followed by rearrangement of the backbone and of the side chain of T75. This suggested that a change involving T75 in one subunit of the KcsA tetramer would lock the SF in a stable nonconducting conformational state with the carbonyl O of T75 coordinating K^+ in site S3 and the amide H, forming a bond with the carbonyl O atom of E71. However, such a transition to a nonconducting state, by rearrangement of the T75-V76 linkage, was not observed in MD analyses based on the GROMOS force field (41). Whereas flipping of the V76-G77 peptide bond was seen, it involved neither a change in the T75-V76 linkage nor a blockage of the SF (41). Earlier MD studies of K^+ permeation in KcsA (42) also indicated that all four Os of T75 continue to coordinate K^+ throughout its transition from site S3 to S4. A recent ab initio study (33) of amino acids near the intracellular entrance to the SF, stressing the carbonyl Os of T75 as a key to alkali metal ion discrimination, indicated that the T75 residues remain fairly close to their x-ray positions in the presence of K^+.

Our minimization results show that the T75-V76 peptide linkage remains undistorted even for an SF void of ions and waters (Fig. 5). The carbonyl Os of T75 remain pointed toward the pore axis. We find that the SF backbone is deformed from residues V76 to the extracellular vestibule. The SF stabilizes itself in this new configuration. The highly conserved residues G77 and G79 permit backbone peptide plane rotations. H-bonding to carbonyl Os from adjacent P-loops effectively stabilizes the unusual conformation, with its flipped peptide planes in the middle of the SF. Experiments have shown that slow inactivation involves rearrangement of the outer mouth of the channel and the extracellular portion of the SF (10,11,43). Our results, as well as experimental evidence (44), suggest that the conformational changes associated with inactivation are localized to the more external binding sites. Site S4 and probably S3 (carbonyl O atoms of T75 and V76) persist in the inactivated state (44), and the H-bonding network between amide Hs and carbonyl Os at the extracellular portion of the SF prevents the passage of ions. Consistent with these observations, we find that the intracellular parts of the SF P-loops (the T75-V76 peptide plane) are rigid in comparison to the extracellular parts. The rigidity arises from the E71-T75 polypeptide chain, forming a tightly packed loop. In this peptide loop, amide Hs of V76 and T75 are stabilized by carbonyl Os of E71 and T72 (in Figs. 2 and 3 the H-bond between the amide H of V76 and carbonyl O of E71 is shown as *dashed line 1*). There is no general collapse of the SF pore (45). Thus we suggest that when the SF is in an inactivated state, the recovery due to K^+ ions entering from the cytoplasm could involve reforming the conductive conformation of the SF's extracellular domain by disrupting the H-bonding network between the P-loops. It should be noted that recovery from the inactivated state for the E71A mutant (Fig. 5 *b*) would be easier because its extracellular SF region is far less deformed.

The low-[K^+] x-ray structure (13) indicates that the V76-G77 amide planes are distorted simultaneously in all four subunits, challenging the MD predictions of reorientation of a single carbonyl group in one subunit. Furthermore, experimental data show that slow inactivation results from a cooperative conformational change involving all four channel subunits (45,46), one directly related to K^+ occupancy of the SF (47). While K^+ ions occupy the SF, constriction cannot take place. When the SF is unoccupied, constriction occurs and inactivation proceeds. Single-channel current traces of open-state KcsA demonstrate rapid, large amplitude fluctuations (2), which imply depletion of K^+ ions in the pore that could be inactivating. Under extreme conditions where the electrochemical gradient removes K^+ ions from the SF faster than they can reenter from the cytoplasm (48), the SF becomes unstable because of reduced K^+ occupancy, and current is interrupted, showing fast flickering. Our results (Fig. 5) strongly suggest that the inactivated state corresponds to conformations with a partially unoccupied or an entirely empty SF. The SF completely void of ions and waters (49) undergoes a conformational change involving all four P-loops, and the new nonconducting conformation is effectively stabilized by H-bonds between amide Hs and carbonyl Os from adjacent P-loops.

The conformational states of the SF observed in MD simulations can be characterized as local structural rearrangements involving only one distorted carbonyl O in one of the four monomers, thus breaking the symmetry of the tetrameric channel (4). The MD-based explanation for a nonconductive SF is based on comparing binding free energy differences for K^+ ions located at specific binding sites with unflipped and flipped carbonyl groups. The experimental evidence supporting this MD interpretation is the observation of a flipped E71A crystal structure with its displaced binding sites and flipped carbonyl groups, which it is tempting to associate with an intermediate conductive conformation in WT-KcsA (6). However, K^+ conduction requires concerted translocation of K^+ and water molecules between SF binding sites. During K^+ translocation, its coordination environment changes continually. Consequently, flipping carbonyl Os could well be a natural feature associated with formation and disruption of specific K^+-water-protein complexes along the SF pore during ion permeation. Only by artificially constraining the carbonyl groups of the SF (39), thus suppressing flipping and distorting a realistic permeation picture, was it possible to observe K^+ conductance in simulation. Finally, the timescale for local peptide backbone atomic motions is ~1 ns (50), i.e., an order of magnitude shorter than the K^+ translocation time under a transmembrane potential of 100 mV, ~10–20 ns (2); the latter is comparable to typical MD simulation times. However, SF inactivation dynamics oper-

ate on a quite different timescale. KcsA inactivation requires hundreds of milliseconds (5), much longer than that accessible via MD simulation. It is thus uncertain whether a SF conformation involving local reorientation of two peptide linkages (T75-V76 and V76-G77) in a single subunit (4) can stabilize a nonconducting state for hundreds of milliseconds, as needed for slow inactivation.

In sum, there is considerable theoretical evidence that carbonyl flipping is an ordinary fluctuation (4,37–41), and is not a crucial step in inactivation (6). There are also numerous experimental and independent theoretical studies supporting our proposition that the portion of the SF directly adjacent to the inner vestibule (cavity) is resistant to deformation, that the part of the SF near the periplasmic mouth is relatively deformable (10,11,43,44) and most likely responsible for inactivation, and that this deformation is associated with an empty or partially occupied filter (47–49).

Conformations of the SF loaded with Na^+

Na^+/K^+ specificity plays a crucial role in many biochemical processes. Both ions carry the same charge and differ only in size (the Na^+ crystal radius is ~0.38 Å less than that of K^+). Neutron and x-ray diffraction studies demonstrate that, when hydrated, Na^+ and K^+ behave very differently (for an extended literature discussion of relevant experimental and theoretical data, see Collins et al. (51) and references therein). The crucial differences are: 1), the Na^+-O distance lags and the K^+-O distance exceeds the O-O separation in pure water, indicating that Na^+ is strongly hydrated and K^+ weakly so; 2), compared with direct interwater coupling, Na^+-water interaction is strong and K^+-water interaction is weak, indicating substantial charge transfer to solvent for Na^+; 3), adjacent waters are strongly oriented by Na^+ but not by K^+; and 4), Na^+ averages 0.25 tightly bound, immobilized waters while those associated with K^+ are constantly being exchanged during aqueous diffusion. Both neutron and x-ray diffraction indicate that only tightly bound water is strongly oriented and that long-range electric fields generated by aqueous Na^+ or K^+ (distances >5 Å) are swamped by direct water-water interactions. Differences in the water affinity of Na^+ and K^+ therefore reflect surface charge density effects, not long-range electric fields (51). Upon entering a narrow SF, ions partially lose their inner water shields, exacting an energetic cost. Because K^+ is relatively chaotropic, when it accesses the SF it ''frees up'' its nearby waters far more easily than Na^+; the kosmotrope hangs on to its tightly bound water molecules. Filter carbonyl ligands have limited reorientational freedom and do not diffuse with the ions; thus the SF matrix more easily mimics the potassium ion's aqueous environment. In sum, binding to SF moieties must provide compensatory stabilization, and selectivity is the consequence of this energetic balancing act.

The physical origin of potassium channel selectivity is currently a matter of great controversy. There are at least four rather different ways to physically account for the differential energetics: 1), Selecting between K^+ and Na^+ is a consequence of pore geometry (52,53) and ionic hydration thermodynamics. Electrostatic interaction between permeating ions and the surrounding protein does not critically influence discrimination among univalent cations. Instead, the surrounding charged or polar groups catalyze dehydration and control channel conductance (52). The energetic cost of constraining a hydrated K^+ inside a narrow pore is less than the cost of constraining a hydrated Na^+ (53). Consequently, K^+ channels have narrow pores (radius ~1.5 Å), whereas Na^+ channels have wider pores; it is this combination of steric and energetic factors that determines selectivity. 2), Selectivity reflects the difference between ionic hydration energy and ionic interaction energy with a polar binding site in the pore (54,55). In contrast to the previous view, this perspective stresses the influence of the field strength of pore-lining ligands on ion selectivity (64). Ion-ligand interaction energies (reflecting ligand field strength or dipole moment) larger than hydration energies favor selection of ions of smaller crystal radius. Conversely, binding sites with the low ligand field strength select for ions of larger crystal radius. 3), The ''snug-fit'' mechanism postulates that K^+ fits snugly within the SF, but Na^+ is too small to fit tightly enough and dehydrate (56). This proposal implies that carbonyl Os are rigidly fixed and cannot approach the smaller Na^+ closely. The electrostatic energy of Na^+ in the rigid eightfold cages would be much higher than that in solution, and Na^+ cannot enter the SF. 4), The binding site's coordination structure and its extended environment cooperate to control selectivity (57,58). In this ''phase-activated'' interpretation (57), the SF is a quasi-liquid; its 8-coordinate K^+ binding site cannot deform sufficiently to create the 5- or 6-coordinate surroundings favored by Na^+.

Comparing the SF loaded with K^+ and Na^+ in our energy minimization study, we find that 1), the conformation, geometry, and location of binding sites differ significantly with Na^+ in the SF; and 2), the SF narrows in the immediate vicinity of Na^+ (Fig. 6). The native binding sites (S1–S3) comfortably accommodate K^+, but when Na^+ replaces K^+, the site geometries are no longer favorable. The SF rearranges to form new binding sites that comfortably accommodate Na^+, directly coordinating only five Os. The preferred coordination is with a ring of four carbonyl Os and one water, but binding in a deformed eightfold carbonyl O cavity is also observed (Fig. 6 *b*). Thus, cation binding generates structurally different K^+-KcsA and Na^+-KcsA complexes. Coordination of Na^+ by four carbonyl Os and two waters was observed in the binding pockets of the SF using a semi-microscopic model (59). Similar conformations were also found in MD simulations of Na^+ occupied KcsA (60,61). From the radial distribution functions, the mean Na^+-O distances were ~2.36 Å, and K^+-O distances were ~2.85 Å. These fall within ranges observed crystallographically for inorganic salts and take thermal fluctuations into account. Previous authors argued that the SF is blocked by its collapse (i.e., formation of a locally constricted ring of carbonyl Os) around Na^+ ions (61). We confirm this viewpoint,

finding that the cylindrical geometry of an SF with well-organized carbonyl groups, nearly ideal for K^+, is not maintained when Na^+ is present. There is significant distortion, with local contraction around Na^+, releasing ligands not involved in Na^+ coordination and leading to occlusion of the permeation pathway. An SF loaded with a mixture of K^+ and Na^+ could be blocked due to strong binding of the smaller Na^+ and local collapse of the SF around it. The radius of the SF shrinks to little more than ~0.4 Å at its narrowest. Thus, strong binding to Na^+ induces a large local narrowing of the filter. Strong Na^+ binding, filter constriction, and greater energetic and positional fluctuations were observed in a reduced model of the SF (62). Ab initio calculations at the Hartree-Fock level also show that Na^+ ions are much more strongly trapped when inside the filter (63).

Our results argue against SF rigidity (the ''snug-fit'' mechanism) (56). The KcsA SF is flexible and readily accommodates Na^+. We see the SF rearrange with five Os coordinating Na^+ (Fig. 6). Both carbonyl and water Os are liganding and the coordination number has changed. However, the SF is distorted and presumably nonconductive. Our results also argue against the ''field strength'' mechanism (54,55). The physical origin of the strain energy (~5.3 kcal/mol at S2 and smaller values at S1 and S3), favoring K^+ over Na^+, was solely attributed to ''through-space'' electrostatic repulsions between carbonyl O atoms (30,31,64). However, backbone mutations of amide carbonyls to ester carbonyls (significant reducing electronegativity in the SF pore due to the ester moiety's lower dipole moment, 1.7 D vs. 3.5 D for an amide) alter K^+ conduction, but not selectivity (12,65). Biochemical and electrophysiological methods have shown that E71 charge-neutralizing mutations alter the inward conductance without influencing either univalent ion selectivity or outward currents (66). These experiments support earlier theoretical work predicting that no major selectivity changes occur due to altering electrostatics within the pore region (52). A potential problem in the field strength explanation of selectivity is that carbonyl dipole moments exceed those of water; thus, following Eisenman's argument (54), one might expect the KcsA SF to select for Na^+ over than K^+ (see view 2 above). Our results show that carbonyl Os can approach each other and solvate the smaller Na^+ (see the fivefold carbonyl O cavity in Fig. 6 *b*) forming a cavity of the appropriate size. We find that the molecular system with the channel occupied by Na^+ is structurally less favorable (~3.2 kcal/mol per ion, Table 4) than when occupied by K^+, agreeing with predictions that selectivity reflects ''external'' or ''topological'' constraints/forces imposed on an ion-coordinated complex by the channel protein (67). Rather than separating enthalpic and entropic components of the free energy (30,31), we quantify individual components of the total (enthalpic) energy in Table 4. The total energy of the system with Na^+ is, unsurprisingly, far less than that with K^+, agreeing with earlier predictions (60,62). Moreover, the difference in the electrostatic energy per ion mimics that of hydrated ions in bulk solution (Table 4).

In summary, our results show that K^+ selectivity arises primarily from the inability of the SF to completely dehydrate the Na^+, due to structural differences between liquid water and the ''quasi-liquid'' SF matrix. Na^+ requires more flexibility in reorienting and repacking ligands (68). A discussion of the structure of and ion binding to the NaK channel (69) suggested that structural variation arising from differences in amino acid packing around the binding sites accounts for the different ion-binding properties of KcsA and NaK. Comparison between the SFs of KcsA and NaK shows that coordination in the NaK filter (with a well separated binding site at the extracellular mouth, a vestibule in which ions can diffuse but not bind, and two binding sites at the intracellular end of the SF) is more flexible than that in the KcsA filter (four tightly packed binding sites along the filter). Disruption of the well-organized SF matrix and the increased conformational freedom in NaK appear responsible for its nonselective conductance of K^+ and Na^+. Simply put, the SF of NaK can properly coordinate both K^+ and Na^+ without structurally constraining the ligands. Thus, the ''quasi-liquid'' SF structure of KcsA, with its lower effective dielectric constant, cannot provide a Na^+ solvation shell that is energetically equivalent to that of bulk water. The local distortion of the SF around Na^+ extracts an energetic cost. The KcsA SF does provide binding sites of the appropriate size for both K^+ and Na^+, in accord with general principles of selective ion transport (70). However, Na^+-KcsA complexes are energetically disfavored since the SF undergoes a conformational change in collapsing around the smaller Na^+ ions. The Na^+ binding cavity is smaller and the SF deforms, providing five coordinating ligands that favorably cradle Na^+. It is possible for Na^+ ions, at high transmembrane voltages, to permeate through the KcsA SF via a ''punch-through'' mechanism (71). Conformational changes in an SF loaded with Na^+ (Fig. 6) provide clues for how this Na^+ permeation process (72) could occur.

CONCLUSIONS

Previously we found that the SF P-loops are structurally unaffected during intracellular gate opening in KcsA (17). No crucial structural change, possibly inducing slow inactivation, is transduced to the SF domain. Thus, we suggest that the intracellular and SF gates might operate independently. Energy minimization of open-state WT and E71A mutated KcsA under appropriate initial K^+ and water SF occupancies leads to well-tuned, clearly identifiable SF conformations that agree well with available crystallographic structures. Even though energy minimization ignores thermal fluctuations, our results also concur with numerous MD-based predictions: reorganization and flipping of carbonyl groups (4,37,38,40), H-bonded interaction between E71p and D80 side chains (22,36,73), a significantly distorted and widened SF at site S1 with both E71 and D80 side chains charged (22,27), and structurally different Na^+-KcsA complexes in Na^+ occupied KcsA (60–62). Since MD studies show that thermal effects do not affect selectivity (62,68), we can have confidence in conclusions based on energy minimization.

We find that the SF completely void of ions and waters undergoes a conformational change involving all four P-loops. Structural modifications are localized to the outer binding sites with site S4 remaining basically unaffected. The nonconducting SF is stabilized by a H-bond network between amide Hs and Os from adjacent P-loops. We suggest that the inactivated state corresponds to this conformation with a partially unoccupied or an entirely empty SF.

The total energy of the system loaded with Na^+ is, as expected, significantly lower than that loaded with K^+. Carbonyl O atoms approach each other and solvate the smaller Na^+, forming an appropriately sized 5-coordinate cavity. However, Na^+-KcsA complexes are energetically disfavored since the SF undergoes substantial structural reorganization in collapsing locally around the smaller Na^+ ions. We conclude that K^+ selectivity primarily arises from the SF's inability to completely dehydrate Na^+, due to structural differences between liquid water and the ''quasi-liquid'' SF matrix.

Our results argue strongly against both the ''snug-fit'' (mechanism 3) and ''field strength'' (mechanism 2) explanations for ion selectivity in the KcsA filter. The KcsA SF is deformable and carbonyl Os can rearrange to coordinate smaller Na^+, providing the proper coordination number and appropriate cavity size. Our results support mechanism 1 deduced from minimalist molecular models in that the charged and polar groups in the pore are not the major determinants of ionic selectivity among ions with the same valence. The predictions of mechanism 4 are also supported by our data in that the SF structure of KcsA is a ''quasi-liquid'' matrix and its distortion around smaller Na^+ to form a fivefold coordination number exerts a structural energetic cost.

SUPPLEMENTARY MATERIAL

To view all of the supplemental files associated with this article, visit www.biophysj.org.

Note added in proof: Recently, isothermal titration calorimetry and x-ray crystallography (three structures of ion-bound and ion-free conformations were determined) were used to establish if size or charge density is recognized by the K^+ channel (74). The channel was more sensitive to ion size than electric field strength, reflecting the influence of protein atoms both near to and far away (as far as 15 Å) from the ion binding sites. With only Na^+ in solution, the channel was found to enter a nonconductive conformation rather than binding Na^+ (74). Thus, discrimination reflects influences from the whole selectivity filter structure, not only intrinsic properties of nearby carbonyls (64). Protein structure is very important to create binding sites that are appropriately sized for K^+ and not for Na^+ (74).

This work was supported by grant GM-28643 from the National Institutes of Health.

REFERENCES

1. Doyle, D. A., J. M. Cabral, R. A. Pfuetzner, A. Kuo, J. M. Gulbis, S. L. Cohen, B. T. Chait, and R. MacKinnon. 1998. The structure of the potassium channel: molecular basis of K^+ conduction and selectivity. *Science*. 280:69–77.
2. LeMasurier, M., L. Heginbotham, and C. Miller. 2001. KcsA: it's a potassium channel. *J. Gen. Physiol.* 118:303–314.
3. Boiteux, C., S. Kraszewski, C. Ramseyer, and C. Girardet. 2007. Ion conductance vs. pore gating and selectivity in KcsA channel: modeling achievements and perspectives. *J. Mol. Model.* 13:699–713.
4. Berneche, S., and B. Roux. 2005. A gate in the selectivity filter of potassium channels. *Structure*. 13:591–600.
5. Gao, L. Z., X. Q. Mi, V. Paajanen, K. Wang, and Z. Fan. 2005. Activation-coupled inactivation in the bacterial potassium channel KcsA. *Proc. Natl. Acad. Sci. USA*. 102:17630–17635.
6. Cordero-Morales, J. F., L. G. Cuello, Y. Zhao, V. Jogini, D. M. Cortes, B. Roux, and E. Perozo. 2006. Molecular determinants of gating at the potassium-channel selectivity filter. *Nat. Struct. Mol. Biol.* 13:311–318.
7. Blunck, R., J. F. Cordero-Morales, L. G. Cuello, E. Perozo, and F. Bezanilla. 2006. Detection of the opening of the bundle crossing in KcsA with fluorescence lifetime spectroscopy reveals the existence of two gates for ion conduction. *J. Gen. Physiol.* 128:569–581.
8. Baker, K. A., C. Tzitzilonis, W. Kwiatkowski, S. Choe, and R. Riek. 2007. Conformational dynamics of the KcsA potassium channel governs gating properties. *Nat. Struct. Mol. Biol.* 14:1089–1095.
9. Chakrapani, S., J. F. Cordero-Morales, and E. Perozo. 2007. A quantitative description of KcsA gating I: macroscopic currents. *J. Gen. Physiol.* 130:465–478.
10. Yellen, G., D. Sodickson, T. Chen, and M. E. Jurman. 1994. An engineered cysteine in the external mouth of a K channel allows inactivation to be modulated by metal binding. *Biophys. J.* 66:1068–1075.
11. Liu, Y., M. E. Jurman, and G. Yellen. 1996. Dynamic rearrangement of the outer mouth of a K^+ channel during gating. *Neuron*. 16:859–867.
12. Lu, T., A. Y. Ting, J. Mainland, L. Y. Jan, P. G. Schultz, and J. Yang. 2001. Probing ion permeation and gating in a K^+ channel with backbone mutations in the selectivity filter. *Nat. Neurosci.* 4:239–246.
13. Zhou, Y., J. H. Morais-Cabral, A. Kaufman, and R. MacKinnon. 2001. Chemistry of ion coordination and hydration revealed by a K^+ channel-Fab complex at 2.0 Å resolution. *Nature*. 414:43–48.
14. Jiang, Y., A. Lee, J. Chen, M. Cadene, B. T. Chait, and R. MacKinnon. 2002. The open pore conformation of potassium channels. *Nature*. 417:523–526.
15. Kelly, B. L., and A. Gross. 2003. Potassium channel gating observed with site-directed mass tagging. *Nat. Struct. Biol.* 10:280–284.
16. Shen, Y., Y. Kong, and J. Ma. 2002. Intrinsic flexibility and gating mechanism of the potassium channel KcsA. *Proc. Natl. Acad. Sci. USA*. 99:1949–1953.
17. Miloshevsky, G. V., and P. C. Jordan. 2007. Open-state conformation of the KcsA K^+ channel: Monte Carlo normal mode following simulations. *Structure*. 15:1654–1662.
18. Shimizu, H., M. Iwamoto, T. Konno, A. Nihei, Y. C. Sasaki, and S. Oiki. 2008. Global twisting motion of single molecular KcsA potassium channel upon gating. *Cell*. 132:67–78.
19. Rapaport, D. C. 2004. The Art of Molecular Dynamics Simulation. 2nd ed. Cambridge University Press, Cambridge, UK.
20. Leach, A. R. 2001. Molecular Modelling: Principles and Applications. Prentice Hall, Harlow, England and New York.
21. Miloshevsky, G. V., and P. C. Jordan. 2004. Anion pathway and potential energy profiles along curvilinear bacterial ClC Cl^- pores: electrostatic effects of charged residues. *Biophys. J.* 86:825–835.
22. MacKerell, A. D., Jr., D. Bashford, M. Bellott, R. L. Dunbrack, Jr., J. D. Evanseck, M. J. Field, S. Fischer, J. Gao, H. Guo, S. Ha, D. Joseph-McCarthy, L. Kuchnir, K. Kuczera, F. T. K. Lau, C. Mattos, S. Michnick, T. Ngo, D. T. Nguyen, B. Prodhom, W. E. Reiher III, B. Roux, M. Schlenkrich, J. C. Smith, R. Stote, J. Straub, M. Watanabe, J. Wiorkiewicz-Kuczera, D. Yin, and M. Karplus. 1998. All-atom empirical potential for molecular modeling and dynamics studies of proteins. *J. Phys. Chem. B*. 102:3586–3616.
23. Ogata, S., T. J. Campbell, R. K. Kalia, A. Nakano, P. Vashishta, and S. Vemparalac. 2003. Scalable and portable implementation of the fast multipole method on parallel computers. *Comput. Phys. Commun.* 153: 445–461.
24. Roux, B., and R. MacKinnon. 1999. The cavity and pore helices in the KcsA K^+ channel: electrostatic stabilization of monovalent cations. *Science*. 285:100–102.

25. Hager, W. W., and H. Zhang. 2005. A new conjugate gradient method with guaranteed descent and an efficient line search. *SIAM J. Optim.* 16:170–192.
26. Berneche, S., and B. Roux. 2002. The ionization state and the conformation of Glu-71 in the KcsA K^+ channel. *Biophys. J.* 82:772–780.
27. Guidoni, L., V. Torre, and P. Carloni. 1999. Potassium and sodium binding to the outer mouth of the potassium channel. *Biochemistry.* 38:8599–8604.
28. Humphrey, W., A. Dalke, and K. Schulten. 1996. VMD—visual molecular dynamics. *J. Mol. Graph.* 14:33–38.
29. Carrillo-Tripp, M., H. Saint-Martin, and I. Ortega-Blake. 2003. A comparative study of the hydration of Na^+ and K^+ with refined polarizable model potentials. *J. Chem. Phys.* 118:7062–7073.
30. Noskov, S. Y., and B. Roux. 2006. Ion selectivity in potassium channels. *Biophys. Chem.* 124:279–291.
31. Noskov, S. Y., and B. Roux. 2007. Importance of hydration and dynamics on the selectivity of the KcsA and NaK channels. *J. Gen. Physiol.* 129:135–143.
32. Kebarle, P. 1977. Ion thermochemistry and solvation from gas phase ion equilibria. *Annu. Rev. Phys. Chem.* 28:445–476.
33. Kariev, A. M., and M. E. Green. 2008. Quantum mechanical calculations on selectivity in the KcsA channel: the role of the aqueous cavity. *J. Phys. Chem. B.* 112:1293–1298.
34. Marcus, Y. 1991. Thermodynamics of solvation of ions. Part 5. Gibbs free energy of hydration at 298.15 K. *J. Chem. Soc., Faraday Trans.* 87:2995–2999.
35. Marcus, Y. 1987. The thermodynamics of solvation of ions. Part 2. The enthalpy of hydration at 298.15 K. *J. Chem. Soc. Faraday Trans. I.* 83:339–349.
36. Bucher, D., L. Guidoni, and U. Rothlisberger. 2007. The protonation state of the Glu-71/Asp-80 residues in the KcsA potassium channel: a first-principles QM/MM molecular dynamics study. *Biophys. J.* 93:2315–2324.
37. Capener, C. E., P. Proks, F. M. Ashcroft, and M. S. P. Sansom. 2003. Filter flexibility in a mammalian K channel: models and simulations of Kir6.2 mutants. *Biophys. J.* 84:2345–2356.
38. Domene, C., A. Grottesi, and M. S. P. Sansom. 2004. Filter flexibility and distortion in a bacterial inward rectifier K^+ channel: simulation studies of KirBac1.1. *Biophys. J.* 87:256–267.
39. Khalili-Araghi, F., E. Tajkhorshid, and K. Schulten. 2006. Dynamics of K^+ ion conduction through Kv1.2. *Biophys. J.* 91:L72–L74.
40. Bernèche, S., and B. Roux. 2000. Molecular dynamics of the KcsA K^+ channel in a bilayer membrane. *Biophys. J.* 78:2900–2917.
41. Kóňa, J., M. Minozzi, V. Torre, and P. Carloni. 2007. A gate mechanism indicated in the selectivity filter of the potassium channel KcsA. *Theor. Chem. Acc.* 117:1121–1129.
42. Shrivastava, I. H., and M. S. P. Sansom. 2000. Simulation of ion permeation through a potassium channel: molecular dynamics of KcsA in a phospholipid bilayer. *Biophys. J.* 78:557–570.
43. Ogielska, E. M., and R. W. Aldrich. 1999. Functional consequences of a decreased potassium affinity in a potassium channel pore. Ion interactions and C-type inactivation. *J. Gen. Physiol.* 113:347–358.
44. Ray, E. C., and C. Deutsch. 2006. A trapped intracellular cation modulates K^+ channel recovery from slow inactivation. *J. Gen. Physiol.* 128:203–217.
45. Ogielska, E. M., W. N. Zagotta, T. Hoshi, S. H. Heinemann, J. Haab, and R. W. Aldrich. 1995. Cooperative subunit interactions in C-type inactivation in K channels. *Biophys. J.* 69:2449–2457.
46. Panyi, G., Z. Sheng, L. Tu, and C. Deutsch. 1995. C-type inactivation of a voltage-gated K^+ channel occurs by a cooperative mechanism. *Biophys. J.* 69:896–903.
47. Kiss, L., and S. J. Korn. 1998. Modulation of C-type inactivation by K^+ at the potassium channel selectivity filter. *Biophys. J.* 74:1840–1849.
48. Schroeder, I., and U. P. Hansen. 2007. Saturation and microsecond gating of current indicate depletion-induced instability of the MaxiK selectivity filter. *J. Gen. Physiol.* 130:83–97.
49. Loboda, A., A. Melishchuk, and C. Armstrong. 2001. Dilated and defunct K channels in the absence of K^+. *Biophys. J.* 80:2704–2714.
50. Hille, B. 2001. Ionic Channels of Excitable Membranes, 3rd ed. Sinauer Associates, Sunderland, MA.
51. Collins, K. D., G. W. Neilson, and J. E. Enderby. 2007. Ions in water: characterizing the forces that control chemical processes and biological structure. *Biophys. Chem.* 128:95–104.
52. Laio, A., and V. Torre. 1999. Physical origin of selectivity in ionic channels of biological membranes. *Biophys. J.* 76:129–148.
53. Carrillo-Trip, M., H. Saint-Martin, and I. Ortega-Blake. 2004. Minimalist molecular model for nanopore selectivity. *Phys. Rev. Lett.* 93:168104.
54. Eisenman, G. 1962. Cation selective electrodes and their mode of operation. *Biophys. J.* 2:259–323.
55. Eisenman, G., and R. Horn. 1983. Ionic selectivity revisited: the role of kinetic and equilibrium processes in ionic permeation through channels. *J. Membr. Biol.* 76:197–225.
56. Bezanilla, F., and C. M. Armstrong. 1972. Negative conductance caused by entry of sodium and cesium ions into the potassium channels of squid axons. *J. Gen. Physiol.* 60:588–608.
57. Varma, S., and S. Rempe. 2007. Tuning ion coordination architectures to enable selective partitioning. *Biophys. J.* 93:1093–1099.
58. Varma, S., D. Sabo, and S. B. Rempe. 2008. K^+/Na^+ selectivity in K channels and valinomycin: over-coordination versus cavity-size constraints. *J. Mol. Biol.* 376:13–22.
59. Garofoli, S., and P. Jordan. 2003. Modeling permeation energetics in the KcsA potassium channel. *Biophys. J.* 84:2814–2830.
60. Biggin, P., G. Smith, I. Shrivastava, S. Choe, and M. Sansom. 2001. Potassium and sodium ions in a potassium channel studied by molecular dynamics simulations. *Biochim. Biophys. Acta.* 1510:1–9.
61. Shrivastava, I. H., D. P. Tieleman, P. C. Biggin, and M. S. P. Sansom. 2002. K^+ versus Na^+ ions in a K channel selectivity filter: a simulation study. *Biophys. J.* 83:633–645.
62. Asthagiri, D., L. R. Pratt, and M. E. Paulaitis. 2006. Role of fluctuations in a snug fit mechanism of KcsA channel selectivity. *J. Chem. Phys.* 125:24701–24706.
63. Huetz, P., C. Boiteux, M. Compoint, C. Ramseyer, and C. Girardet. 2006. Incidence of partial charges on ion selectivity in potassium channels. *J. Chem. Phys.* 124:044703.
64. Noskov, S. Y., S. Berneche, and B. Roux. 2004. Control of ion selectivity in potassium channels by electrostatics and dynamic properties of carbonyl ligands. *Nature.* 431:830–834.
65. Valiyaveetil, F. I., M. Sekedat, R. MacKinnon, and T. W. Muir. 2006. Structural and functional consequences of an amide-to-ester substitution in the selectivity filter of a potassium channel. *J. Am. Chem. Soc.* 128:11591–11599.
66. Choi, H., and L. Heginbotham. 2004. Functional influence of the pore helix glutamate in the KcsA K^+ channel. *Biophys. J.* 86:2137–2144.
67. Bostick, D., and C. L. Brooks 3rd. 2007. Selectivity in K^+ channels is due to topological control of the permeant ion's coordinated state. *Proc. Natl. Acad. Sci. USA.* 104:9260–9265.
68. Thomas, M., D. Jayatilaka, and B. Corry. 2007. The predominant role of coordination number in potassium channel selectivity. *Biophys. J.* 93:2635–2643.
69. Shi, N., S. Ye, A. Alam, L. Chen, and Y. Jiang. 2006. Atomic structure of a Na^+- and K^+-conducting channel. *Nature.* 440:570–574.
70. Gouaux, E., and R. MacKinnon. 2005. Principles of selective ion transport in channels and pumps. *Science.* 310:1461–1465.
71. Nimigean, C. M., and C. Miller. 2002. Na^+ block and permeation in a K^+ channel of known structure. *J. Gen. Physiol.* 120:323–325.
72. Kiss, L., J. LoTurco, and S. J. Korn. 1999. Contribution of the selectivity filter to inactivation in potassium channels. *Biophys. J.* 76:253–263.
73. Ranatunga, K. M., I. H. Shrivastava, G. R. Smith, and M. S. P. Sansom. 2001. Side-chain ionization states in a potassium channel. *Biophys. J.* 80:1210–1219.
74. Lockless, S. W., M. Zhou, and R. MacKinnon. 2007. Structural and thermodynamic properties of selective ion binding in a K^+ channel. *PLoS Biology.* 5:1079–1088.